Biogeosciences Discuss., 9, 2655–2689, 2012
www.biogeosciences-discuss.net/9/2655/2012/
doi:10.5194/bgd-9-2655-2012

Biogeosciences Discussions

Effects of seawater pCO_2 changes on the calcifying fluid of scleractinian corals

S. Hohn[1] **and A. Merico**[1,2]

[1]Leibniz Center for Tropical Marine Ecology, Systems Ecology, Fahrenheitstraße 6, 28359 Bremen, Germany
[2]Jacobs University Bremen, School of Engineering and Science, Campus Ring 1, 28759 Bremen, Germany

Received: 14 February 2012 – Accepted: 23 February 2012 – Published: 9 March 2012

Correspondence to: S. Hohn (soenke.hohn@zmt-bremen.de)

Published by Copernicus Publications on behalf of the European Geosciences Union.

Abstract

Rising atmospheric CO_2 concentrations due to anthropogenic emissions induce changes in the ocean carbonate chemistry and a drop in ocean pH. This acidification process is expected to harm calcifying organisms like coccolithophores, molluscs, echinoderms, and corals. A severe decline in coral abundance is, for example, expected by the end of this century with associated disastrous effects on reef ecosystems. Despite the growing importance of the topic, little progress has been made with respect to modelling the impact of acidification on coral calcification. Here we present a model for a coral polyp that simulates the carbonate system in four different compartments: the seawater, the polyp tissue, the coelenteron, and the calicoblastic layer. Precipitation of calcium carbonate takes place in the metabolically controlled calicoblastic layer beneath the polyp tissue. The model is adjusted to a state of activity as observed by direct microsensor measurements in the calcifying fluid. Simulated CO_2 perturbation experiments reveal decreasing calcification rates under elevated pCO_2 despite strong metabolic control of the calcifying fluid. Diffusion of CO_2 through the tissue into the calicoblastic layer increases with increasing seawater pCO_2 leading to decreased aragonite saturation in the calcifying fluid of the coral polyp. Our modelling study provides important insights into the complexity of the calcification process at the organism level and helps to quantify the effect of ocean acidification on corals.

1 Introduction

Rising atmospheric CO_2 concentrations due to fossil fuel emissions and land use changes are well known perturbations to environmental scientists as well as to the general public (IPCC, 2007). Even though there may still be some uncertainties about the absolute amount of CO_2 annually taken up by the oceans, there is general agreement that the oceans take up about a quarter of the CO_2 emitted in a year (Sabine et al., 2004). CO_2 reacts with water to produce carbonic acid that further dissociates

BGD
9, 2655–2689, 2012

by releasing protons. This causes a drop in ocean pH which is therefore a direct consequence of rising atmospheric CO_2 concentrations, a process termed "ocean acidification" (OA) (Caldeira and Wickett, 2003). How these changes in seawater chemistry affect the life of marine organisms is, however, still a matter of debate (Ridgwell et al., 2009; Ries et al., 2009).

Marine organisms that produce skeleton structures of calcium carbonate ($CaCO_3$) are thought to be most susceptible to OA (Doney et al., 2009). This is because precipitation and dissolution of $CaCO_3$ (in the various mineral forms) are strongly dependent on the carbonate ion concentration, which decreases with decreasing pH (Zeebe and Wolf-Gladrow, 2001). There is great concern that tropical coral reefs may be strongly affected by changes in seawater carbonate chemistry as these ecosystems are dominated by many calcifying organisms whose mineralogical remains build up the calcareous sediments in these regions (Cohen and Holcomb, 2009). Even though tropical surface waters will not become undersaturated with respect to aragonite or calcite within the next 100 yr (Orr et al., 2005), the changes in carbonate chemistry are expected to cause a decrease in coral calcification rates of up to 30 %, most probably turning many coral reefs into non-reef coral communities with zero or even negative calcium carbonate accumulation (Kleypas et al., 2001). However, despite oversaturation with respect to aragonite and calcite, spontaneous precipitation of $CaCO_3$ does not occur in the ocean. The formation of $CaCO_3$ crystals in seawater is inhibited by high concentrations of magnesium and phosphate that occupy the binding sites for calcium and carbonate ions on the crystal lattice (Pytkowicz, 1973; Lasaga, 1998).

The fact that marine calcifying organisms like corals precipitate $CaCO_3$ despite the mentioned inhibition mechanisms leads to the conclusion that Mg^{2+} and/or PO_4^{3-} are actively excluded from the calcifying fluid. Furthermore, net calcification (precipitation minus dissolution) only occurs when the ion product of calcium and carbonate exceeds the stoichimetric solubility product of a particular mineral phase (Lasaga, 1998; Zeebe and Wolf-Gladrow, 2001). Calcifying organisms therefore must hold a concentration mechanism for these ions at the site of calcification that concurrently resupplies Ca^{2+}

BGD
9, 2655–2689, 2012

and CO_3^{2-}, which are continuously consumed by calcium carbonate precipitation. The calcifying fluid therefore differs from the growth medium and is usually separated from the seawater by at least two membranes (Allemand et al., 2004).

It has been shown that corals increase the pH in the calcifying fluid with respect to their growth medium (Al-Horani et al., 2003) by actively removing protons from the calcifying fluid (Ries, 2011) and thus increasing its saturation state. The removal of protons is likely connected to the activity of the calcium pump that acts as a proton-calcium antiporter (Gould et al., 1986; Allemand et al., 2004). In this case, the assumption of either a weak or a strong proton pump, or the maintenance of a constant proton gradient in corals (Ries, 2011) has also implications for the calcium transport. However, calcium and protons in the calicoblastic layer are not maintained at fixed concentrations but vary with different light conditions (Marubini et al., 2001; Al-Horani et al., 2003). A study by Ries (2011) recently investigated the calcification response to changing pCO_2 under potential steady state conditions within the coral, without resolving the underlying (short-term) dynamics. The study also assumed equal concentrations of DIC and Ca^{2+} in the calcifying fluid and growth medium, although it has been shown that they may differ at least for the case of Ca^{2+} (Tambutté et al., 1996; Al-Horani et al., 2003).

However, if the calcifying fluid is metabolically controlled by the coral polyp and differs substantially from the growth medium, how and why should precipitation and dissolution of calcium carbonate in the calicoblastic layer be related to external changes in seawater chemistry? To address this question, we developed a mathematical model of coral polyp calcification that computes the kinetic reactions of the carbonate chemistry in four different model compartments (as identified by Tambutté et al., 1996) and is parameterized and constrained with the microsensor experiments of Al-Horani et al. (2003). We investigated the temporal dynamics of calcium and carbon in the coral polyp and the responses of polyp calcification to ocean acidification with perturbed CO_2 concentrations in the simulated growth medium.

BGD
9, 2655–2689, 2012

2 Methods

2.1 Model description

We developed a box model for a coral polyp that comprises the following compartments: the growth medium (seawater), the stomach room of the polyp (coelenteron), the actual body of the coral polyp (tissue), and the calcifying fluid (calicoblastic layer) (Fig. 1). The model resolves the full kinetic reactions of the carbonate system, including boric acid and borate, according to Zeebe and Wolf-Gladrow (2001). The state variables considered in each compartment are: dissolved carbon dioxide (CO_2), bicarbonate (HCO_3^-), carbonate (CO_3^{2-}), protons (H^+), hydroxide ions (OH^-), boric acid ($B(OH)_3$), borate ($B(OH)_4^-$), and calcium ions (Ca^{2+}). Precipitation and dissolution of calcium carbonate ($CaCO_3$) are considered only in the calicoblastic layer and are parameterized according to Zuddas and Mucci (1994). The seawater compartment is connected to an overlying atmosphere via the air-sea gas-exchange of CO_2 (Wanninkhof, 1992). Atmospheric CO_2 concentrations, ambient temperature and seawater salinity, are used as external forcing. State variables in seawater and the coelenteron are assumed to be connected via advective exchange (at constant rate) due to feeding. CO_2 is assumed to freely diffuse from the seawater, the coelenteron, and the calicoblastic layer into the polyp tissue and out again, depending on the concentration gradient and the diffusivity of CO_2 over eukaryotic cell membranes (Sueltemeyer and Rinast, 1996). Calcium transport from the tissue to the calcifying fluid is assumed to be mediated by a Ca^{2+}-H^+-antiporter (Ca-ATPase, Ip et al., 1991; Zoccola et al., 2004) and is parameterized with simple Michaelis-Menten kinetics, depending on calcium concentrations only. The Ca-ATPase is assumed to transport two protons for each calcium ion to assure charge balance. In nature, the entrance of calcium from seawater and the coelenteron into the tissue occurs either passively via Ca^{2+}-channels or actively via a transporter (Allemand et al., 2004). In our model, we only assume active calcium uptake and parameterize the transporter in the same way as for calcium

BGD
9, 2655–2689, 2012

excretion into the calicoblastic layer. A bicarbonate transporter (co-transport of HCO_3^- and H^+) is also considered for active carbon uptake from the seawater and the coelenteron into the tissue and transport from the tissue into the calicoblastic layer (Furla et al., 2000). The bicarbonate transporter is parameterized with Michaelis-Menten kinetics on HCO_3^-. Photosynthesis and respiration are considered as source and sink of CO_2 in the polyp tissue and the rates are taken from the experiments of Al-Horani et al. (2003). Model equations are given in the Appendix.

2.2 Model runs

As primary reference for our simulations, we used data of the microsensor experiments by Al-Horani et al. (2003), in which calcium ion concentrations and pH were measured at the polyp surface, in the coelenteron and in the calicoblastic layer beneath the coral tissue. In these experiments, the time evolution of calcium ion concentrations and pH was measured during coral exposure to light and darkness for different time periods. Even though the study by Al-Horani et al. (2003) presents a unique and valuable dataset, the data were not obtained simultaneously due to limitations in the methodology and thus belong to different experiment runs at different times and for different time intervals. In our model, however, all concentrations are determined simultaneously thus allowing investigations of direct interactions and interdependencies of state variables in the model compartments. The model is set up to obtain the best representation of calcium ion concentrations in the calicoblastic layer (Fig. 2d), as this is one of the most relevant aspects to coral calcification.

The simulation is run for 1260 s with a time step of 6×10^{-4} s. Light periods are from 0–420 s and from 840–1260 s. The dark period is from 420–840 s integration time as in the experiment for calcium ion measurements in the calicoblastic layer (Al-Horani et al., 2003, Fig. 2). Active transport of calcium and bicarbonate as well as consumption of CO_2 due to photosynthesis are assumed to occur in the light period only. In the dark, CO_2 is produced in the coral tissue by respiration.

BGD
9, 2655–2689, 2012

Al-Horani et al. (2003) used the coral *Galaxea fascicularis* in their study, a species with rather large polyps. The sizes of the polyp compartments required by the model are obtained by assuming spherical geometry of the polyp with densest sphere packing of polyps within the colony. The diameter of a *G. fascicularis* polyp was estimated to be approximately 8.2 mm (Leuzinger et al., 2003). The volume of the above seawater medium was set to 1 m^3. Seawater temperature was 20.5 °C and salinity was 40 psu during the experiments (Al-Horani et al., 2003).

2.3 Model scenarios

After having defined a set of parameter values (Table 2) and initial conditions (Table 1) with which the model adequately represents the observations, we repeated the model simulations for different atmospheric pCO_2 to determine the effect of changing seawater chemistry on the calcification rate of the simulated polyp. The carbonate chemistry in the seawater compartment is then initialized in equilibrium with the atmosphere at CO_2 partial pressures of 280, 380, 700, and 1000 ppmv (Table 3). The initial values of the other state variables and other parameters were set according to the reference run (Tables 1 and 2).

3 Results

Even though the model resolves the time evolution of the full set of state variables, i.e. all components of the carbonate system, we summed up carbon dioxide, bicarbonate, and carbonate and considered total dissolved inorganic carbon (DIC) to simplify the analysis of the model results. Bicarbonate, carbonate, hydroxide ions, protons and borate are combined to calculate total alkalinity (TA) in all model compartments (Wolf-Gladrow et al., 2007). pH is determined from proton concentrations. As pH data were obtained from experiments with slightly different time intervals than for the determination of calcium ion concentrations, we shifted the pH data on the time axis to match the switches in light conditions in the simulation (Fig. 3c,d).

BGD
9, 2655–2689, 2012

3.1 Seawater

In the model, the metabolic activity of the coral has hardly any influence on seawater composition because the volume of the seawater compartment is much larger than the polyp and the fluxes are negligible compared to the large reservoir of the growth medium. Concentrations of state variables in the seawater compartment therefore do not change over time (Figs. 2–5a).

3.2 Coelenteron

Active uptake of calcium in the light period decreases calcium ion concentrations in the coelenteron (Fig. 2c). During dark phases, calcium is resupplied via advective water exchange between the coelenteron and the seawater compartment so that its concentration is restored towards background values (10 mmol kg^{-1}). As the uptake of calcium into the coral tissue is parameterized as an anti-transport with protons, one might expect the removal of calcium ions from the coelenteron to also decrease the pH in the coelenteron due to the proton efflux. However, the opposite is observed in the data as well as in the model simulations (Fig. 3c). The pH increase in the light phase is due to the decrease of the CO_2 concentration in the coelenteron, as it can also be observed in the DIC concentrations (Fig. 4c), the reason being photosynthetic carbon fixation and successive CO_2 diffusion from the coelenteron into the tissue. Respiration and advective exchange with the seawater restore pH and DIC in the coelenteron towards background values during the dark phase. The proton flux into the coelenteron, however, decreases total alkalinity in the coelenteron during light exposure (Fig. 5c). In the dark, coelenteron alkalinity relaxes towards seawater alkalinity due to water exchange as previously described for the calcium concentrations.

BGD
9, 2655–2689, 2012

3.3 Tissue

In the simulated coral tissue, calcium ion concentrations increase during the light period (Fig. 2b). This is because active uptake of calcium from seawater and coelenteron is currently higher than calcium transport from the polyp tissue to the calicoblastic layer. The rate of calcium uptake has been chosen to match the decrease of calcium concentrations in the coelenteron during light exposure. The maximum calcium transport rate into the calicoblastic layer has been defined to match the increase of calcium concentrations in the calcifying fluid, in addition to the effects of aragonite precipitation and dissolution. Thus, calcium concentrations increase in the tissue as the simulation progresses with time (Fig. 2b). It could be expected that uptake and outflow are balanced in the coral polyp and that intracellular calcium concentrations equilibrate around a certain value. However, this model compartment cannot be appropriately constrained, as no data on intracellular calcium concentrations are available. The changes of intracellular pH in the coral tissue (Fig. 3b) are mainly driven by photosynthesis and respiration, which change intracellular CO_2 concentrations and thus DIC in the tissue (Fig. 4b). Intracellular pH mainly responds to changes in the carbonate chemistry. However, the imbalance between calcium uptake and calcium transport to the calicoblastic layer can also be recognized in the total alkalinity (Fig. 5b) as the calcium-proton anti-transport is reflected in a slight increase of pH in the polyp tissue. As all active transporters are assumed to operate during light exposure only, no changes of intracellular calcium concentrations or alkalinity are observed in the dark (Figs. 2 and 5b).

3.4 Calicoblastic layer

Four processes influence state variables in the calicoblastic layer: 1) diffusion of CO_2, 2) HCO_3^--transport, 3) Ca^{2+}-transport, and 4) calcification (mineralization). Active transport of calcium from the tissue to the calicoblastic layer increases calcium concentrations in the calcifying fluid during light exposure (Fig. 2d). Calcium transport concurrently removes protons from the calcifying fluid, thus also increasing pH and

BGD
9, 2655–2689, 2012

total alkalinity (Figs. 3 and 5d). In the darkness, calcium transport is stopped and calcium ions are removed from the fluid and transferred to the mineral phase. As the mineralization of aragonite also removes carbonate from the calcifying fluid, this process decreases total alkalinity and DIC (Figs. 4 and 5d).

The transport of bicarbonate to the calcifying fluid increases total DIC in the light phase (Fig. 4d). CO_2 diffusion, however, works in both directions, from the calicoblastic layer into the polyp tissue and vice versa. In the light, photosynthesis fixes CO_2 in the polyp tissue and creates a gradient that draws CO_2 from the calicoblastic layer into the polyp tissue. In the darkness, respiration reverses this gradient and CO_2 diffusion resupplies DIC to the calcifying fluid despite absence of active bicarbonate transport (Fig. 4d). Since diffusion is driven by a concentration gradient, the gradual changes in CO_2 concentrations after the light switches produce a time lag or gradual shift in diffusion rates. In addition to the calcium-proton anti-transport, the pH in the calcifying fluid also responds to CO_2 diffusion, increasing pH in the light and decreasing in the dark.

3.5 Calcification over time

With the model it is possible to investigate the dynamics of aragonite precipitation in the calcifying fluid over time (Fig. 6). The light dependent metabolic activity of the coral polyp (i.e. the active transport of calcium and bicarbonate, the removal of protons, and the suction of CO_2 to the site of photosynthesis) increases the concentrations of calcium and carbonate ions in the calcifying fluid and thus increases the saturation state for calcium carbonate. Precipitation and dissolution of aragonite only depend on the aragonite saturation in the calcifying fluid (Eq. A11). The increase of the calcification rate during light exposure, as shown in Fig. 6, is therefore the result of the active metabolic regulation of the ion composition in the calcifying fluid. Only when light is switched off and the ion transport mechanism is inactive, mineralization of aragonite depletes calcium and carbonate and the calcifying fluid approaches equilibrium with the mineral phase (Fig. 6). CO_2 diffusion due to respiration of the polyp, however, still

BGD
9, 2655–2689, 2012

acts as a source of DIC to the calicoblastic layer in the dark, thus never allowing the calcifying fluid to reach the equilibrium with the mineral phase. Calcification occurs at variable rates between 0 and 15 mmol Ca m^{-2} d^{-1} (Fig. 6).

At the end of the light period, the calcification rate exceeds the transport rate of calcium ions and the calcium concentration in the calicoblastic layer decreases before light is switched off (Fig. 2d). The same response can be observed for total alkalinity (Fig. 5d). This decrease at the end of the light period is even more pronounced for DIC concentrations (Fig. 4d). This is because CO_2 diffusion into the polyp tissue adds to calcification as a carbon sink and both sinks altogether become higher than bicarbonate transport as the single carbon source to the calcifying fluid. Only the pH in the calicoblastic layer does not decrease before the onset of the dark period. This is because the pH changes due to diffusion of CO_2 into the polyp tissue are higher than the calcium-proton anti-transport (Fig. 3d).

3.6 Calcification over pCO_2

Since the main intention of this study is to investigate how changes in the carbonate chemistry of the growth medium actually affect coral polyp calcification in the calicoblastic layer, we performed pCO_2 perturbation experiments at pCO_2 levels of 280, 380, 700, and 1000 ppmv. For each scenario, we have calculated the average calcification rates over the simulation period (Fig. 7). Average coral polyp calcification decreases with increasing pCO_2 in the growth medium (Fig. 7) as also observed in experimental studies (Marubini et al., 2008).

In the model, the calcifying fluid is not directly connected to seawater and we assume no active transport of CO_3^{2-}. Hence, the decrease of polyp calcification with increasing pCO_2 cannot be explained by the decrease of carbonate ion concentrations (i.e. lower saturation state) in the seawater compartment. The modelled saturation state in the calicoblastic layer, however, decreases with increasing pCO_2. The relative decrease in carbonate ion concentrations in the calcifying fluid is caused by elevated diffusion of CO_2 from seawater through the coral tissue into the calicoblastic layer.

BGD
9, 2655–2689, 2012

4 Discussion

4.1 Sensitivity of coral calcification to ocean acidification

This study addresses the questions of how and why coral calcification is influenced by the pCO_2 changes in the growth medium. The answers are not straightforward because: 1) the calcifying fluid is separated from seawater by the polyp tissue, and 2) the ion composition of the calcifying fluid is metabolically controlled. Our model, however, shows a decline in coral polyp calcification with increasing seawater pCO_2 (Fig. 7), as also observed by experimental studies (Marubini et al., 2008). This result, together with the good representation of the short-term lab-experiments of Al-Horani et al. (2003), suggests that the model is based on reasonable assumptions. It should be noted that the model does not include a direct dependence of calcification on seawater saturation state or carbonate ion concentrations. The connection between the calcifying fluid and the growth medium is realized via free diffusion of CO_2 over cell membranes and through the cells of the polyp tissue. Additionally to CO_2 diffusion, we considered a bicarbonate transporter from the seawater into the tissue and from the tissue to the calicoblastic layer as has been proposed by Furla et al. (2000). Parallel to elevated CO_2 diffusion from the growth medium to the calcification site, bicarbonate transport slightly increases with rising pCO_2 as also the bicarbonate concentration in seawater increases. When calcium transport to the calcification site is fixed in the different scenarios, the increased supply of CO_2 and HCO_3^- changes the carbonate chemistry in the calcifying fluid and decreases the concentration of carbonate ions, ultimately altering the overall calcification rate (Fig. 7).

The basic physiological mechanisms and pathways considered in the model are based on first principles and chemical reaction kinetics. On very short time scales therefore the model reproduces the experiments by Al-Horani et al. (2003) with good accuracy. The inorganic carbonate chemistry is not affected by major uncertainties (Zeebe and Wolf-Gladrow, 2001; Riebesell et al., 2009) and even the pathways for calcium transport in corals are relatively well understood (Ip et al., 1991; Allemand et al.,

BGD
9, 2655–2689, 2012

2004; Zoccola et al., 2004). The pathway for carbon transport to the calicoblastic layer is still, however, a matter of debate (Marubini et al., 2008), albeit Furla et al. (2000) have proposed the involvement of an anion exchanger.

Since CO_2 diffusion over cell membranes is a passive process, the observed pCO_2 dependence of calcification should be common to other calcifying organisms as well. However, Ries et al. (2009) have shown a huge variability of the pCO_2 response of calcification for different marine calcifiers. These calcification responses range from linear increase with aragonite saturation over saturating increase and an "optimum curve" to linearly decreasing calcification with increasing Ω. Metabolic activity, i.e. respiration and photosynthesis, strongly affects the pCO_2 in the microenvironment of the calcification site and the transport rates of calcium and bicarbonate into the calcifying fluid are most likely not the same for all organisms (Ries, 2011). Our model has been parameterized for a specific experiment with a single coral species and we would expect slightly different parameter values for different species or organisms.

4.2 Carbon supply to the calicoblastic layer

Even though elevated CO_2 diffusion at elevated seawater pCO_2 may explain the decrease in coral polyp calcification, this process alone is not sufficient to sustain calcification in the calicoblastic layer. When in the model CO_2 diffusion is considered to be the only carbon source to the calicoblastic layer, we find that calcium carbonate precipitation depletes DIC to very low concentrations and calcification rates become very low. This result is consistent with the decrease in calcification rates when anion exchangers in coral polyps are inhibited (Furla et al., 2000). Calcification thus becomes carbon limited and calcium ions accumulate to unrealistically high concentrations. We therefore propose that CO_2 diffusion alone is not sufficient to sustain observed calcification rates and that an additional pathway for carbon transport to the calicoblastic layer has to exist.

Our conclusion is supported by the fact that the model correctly reproduces the observed changes in calicoblastic layer pH and calcium ion concentrations (Figs. 2 and 3)

BGD
9, 2655–2689, 2012

and shows a sustained calcification only when bicarbonate transport in symport with protons is assumed. In principle, these observations might be appropriately reproduced also by assuming a carbonate ion transporter, but a bicarbonate transporter is much more likely (see also Furla et al., 2000). Regardless of the actual ion involved, our study shows that an active carbon transport mechanism has to exist.

When calcification increases during the light period, the carbon sinks exceed carbon supply and DIC concentrations in the calicoblastic layer decline already way before light is switched off (Fig. 4d). Maintaining of continuous calcification is therefore the result of a fragile interplay between carbon supply and calcium-proton anti-transport in the coral polyp.

4.3 Model-data comparison

The model qualitatively reproduces the observed time evolution of calcium concentrations and pH in the calicoblastic layer and in the coelenteron (Figs. 2 and 3). Deviations between the model and the data can be explained as follows.

The simulated changes of calcium concentrations in the calicoblastic layer are slightly steeper and more pronounced than in the data, whereas the amplitude in the pH-signal is not as high as in the data. A way for the corals to dampen changes in calcium concentrations in the calicoblastic layer could be to decrease the maximum calcium transport rate but this would also reduce the changes in pH. Since pH is strongly affected by variations in the carbonate chemistry, the most plausible explanation for the models underestimation of the changes in pH and the slight overestimation of the changes in calcium concentrations is probably connected with DIC and TA. The buffering capacity of the calcifying fluid may be too high to allow pH to vary in the same range as in the measured data. Unfortunately, no direct observations are available on DIC and TA in the calcifying fluid. Our model is highly sensitive to DIC and TA in the calcifying fluid and therefore provides reasonable constraints to inversely calculate what DIC concentrations and TA must have been in the calicoblastic layer in order to explain the observed changes of $[Ca^{2+}]$ and pH. This, however, would be valid if the observed

BGD
9, 2655–2689, 2012

variables were consistent to each other, but as explained, the measurements do not belong to the same experimental runs.

In the coelenteron, the simulated pH is overestimated with respect to the observations, although the general pattern (i.e. increasing pH during light exposure and decreasing pH in darkness) is correctly reproduced. The deviations might be explained by the effects of digestive enzymes on the pH of the coelenteron, which are not considered in the model. The small discrepancy in the amplitude might be due to differences in time intervals of the light switches as the general shape of the modelled curve corresponds well with the observations. However, concentration changes of state variables in the stomach compartment are also sensitive to polyp geometry. The polyp geometry assumed in the model defines the volume of the coelenteron and the surface areas especially for the diffusive fluxes. The smaller this volume, the larger the concentration changes for the defined fluxes. Unfortunately, the size of this compartment has not been determined by Al-Horani et al. (2003), we therefore used estimates from other studies (Leuzinger et al., 2003).

We argue that the model qualitatively reproduces the observed responses of measured calcium and hydrogen ions to changing light climate.

4.4 Metabolic regulations and temperature

The controlled conditions in Al-Horani et al. (2003)'s experiments and the actual observations represent strong constraints for our model. The composition of the seawater medium and temperature did not change over investigation time and light was simply switched on and off without altering the light intensity. In the model, these conditions are simulated by simply changing between photosynthetic CO_2 fixation in the light and respiratory CO_2 production in the dark. Active ion transport is assumed to take place only during light exposure. This is of course a simplification. While irradiance instantaneously triggers photosynthesis in the symbiotic zooxanthellae (Gattuso et al., 1999), the metabolic "machinery" of the coral polyp will most probably react gradually to abrupt changes in light conditions (Furla et al., 2000). This might be taken into

BGD
9, 2655–2689, 2012

account by resolving metabolic regulations of the coral polyp, for example by considering a dynamic energy pool that controls the activity of ion transport proteins and/or variable pools of functional proteins and energy-rich metabolites. Dynamic energy pools might lead to an improved representation of the data and improve the model's ability to predict the coral's response to combined changes in environmental conditions such as light, temperature, nutrition, and carbonate chemistry (Kleypas et al., 1999). These pools are, however, extremely difficult to constrain due to the lack of data.

The nutritional status of a coral probably also affects the metabolic activity and thus ion transport in the polyps. In our model we could observe that the activity of the ion transporters strongly affects the calcification rate of the coral polyp (Fig. 6). The experiments by Al-Horani et al. (2003), and thus also our simulations, are run over a short time period, in which the protein content of the polyp can be assumed to remain unchanged. The nutritional status of the coral is therefore not relevant in this study.

The interaction between the polyp host and the algal symbionts may also become more important when considering temperature effects on coral calcification. High temperatures induce the rejection of symbionts by the polyp, a process known as coral bleaching (Iglesias-Prieto et al., 1992; Anthony et al., 2008). Changing temperatures will also affect the speed of the reactions in the carbonate system and possibly the activity of polyp enzymes and the respiration processes (Marshall and Clode, 2004). Since ocean acidification is expected to co-occur in concert with global warming, studies aiming at understanding the combined effects of changing temperature and seawater carbonate chemistry are highly desirable.

5 Conclusions

Our modelling study is a mechanistic investigation of coral physiology and potential pathways of ion transport to the calcification site. We showed that CO_2 diffusion to the calicoblastic layer alone is not sufficient to sustain the observed calcification rates. An additional pathway is required to transport carbon into the calcifying fluid, which we propose to be represented by a bicarbonate transporter (Furla et al., 2000).

BGD
9, 2655–2689, 2012

Our model shows that the decrease in coral calcification with raising seawater pCO_2 is a result of increased diffusion of CO_2 through the polyp tissue to the calcification site and may not depend on the abundance of carbonate ions in the growth medium as proposed, for example, for coccolithophores (Gehlen et al., 2007). The model further provides additional information on changes in DIC and TA occurring in the calcifying fluid that could not be obtained otherwise.

Appendix A

Model equations

A The model equations can be generalised as follows:

$$y(t) = \boldsymbol{v}(t) \quad \text{(A1)}$$

$$y'(t) = \boldsymbol{f}(t) \quad \text{(A2)}$$

$$\boldsymbol{f}(t) = \mathbf{M} \times \boldsymbol{r}(t) \quad \text{(A3)}$$

where $\boldsymbol{v}(t)$ is the vector of state variables, $\boldsymbol{f}(t)$ is the flux vector, that is defined by the product of the reaction vector, $\boldsymbol{r}(t)$, in which all single reactions are mathematically defined, and the flux matrix, $\mathbf{M}$, in which the reactions are assigned to the state variables and, under consideration of compartment volumes and surface areas, are summarized to the net fluxes, i.e. the time derivatives, $y'(t)$, of the function, $y(t)$, to be solved.

BGD
9, 2655–2689, 2012

A1 State variables

State variables are defined as follows.

$$v_{(1:8)} = \begin{bmatrix} CO_{2(sea)} \\ HCO^{-}_{3(sea)} \\ CO^{2-}_{3(sea)} \\ H^{+}_{(sea)} \\ OH^{-}_{(sea)} \\ H_2O_{(sea)} \\ B(OH)^{-}_{4(sea)} \\ B(OH)_{3(sea)} \\ Ca^{2+}_{(sea)} \end{bmatrix}; \quad v_{(9:16)} = \begin{bmatrix} CO_{2(coel)} \\ HCO^{-}_{3(coel)} \\ CO^{2-}_{3(coel)} \\ H^{+}_{(coel)} \\ OH^{-}_{(coel)} \\ H_2O_{(coel)} \\ B(OH)^{-}_{4(coel)} \\ B(OH)_{3(coel)} \\ Ca^{2+}_{(coel)} \end{bmatrix}$$

$$v_{(17:24)} = \begin{bmatrix} CO_{2(tiss)} \\ HCO^{-}_{3(tiss)} \\ CO^{2-}_{3(tiss)} \\ H^{+}_{(tiss)} \\ OH^{-}_{(tiss)} \\ H_2O_{(tiss)} \\ B(OH)^{-}_{4(tiss)} \\ B(OH)_{3(tiss)} \\ Ca^{2+}_{(tiss)} \end{bmatrix}; \quad v_{(25:33)} = \begin{bmatrix} CO_{2(cali)} \\ HCO^{-}_{3(cali)} \\ CO^{2-}_{3(cali)} \\ H^{+}_{(cali)} \\ OH^{-}_{(cali)} \\ H_2O_{(cali)} \\ B(OH)^{-}_{4(cali)} \\ B(OH)_{3(cali)} \\ Ca^{2+}_{(cali)} \\ CaCO_{3(cali)} \end{bmatrix} \tag{A4}$$

The indices (sea), (coel), (tiss), and (cali) refer to the compartments of seawater, coelenteron, tissue, and calicoblastic layer, respectively.

BGD
9, 2655–2689, 2012

A2 Reactions

The chemical reactions of the carbonate system in seawater are calculated according to Zeebe and Wolf-Gladrow (2001) using 14 equations with 14 reaction rates, k, of the back, −, and forward, +, reactions. The reaction rates are assigned as described in Table 2.3.1, p. 110, in Zeebe and Wolf-Gladrow (2001). The carbonate chemistry is calculated in each model compartment. For reactions 1–14, the index of the involved chemicals refers to the seawater compartment, (i) = (sea), whereas for reactions 15–28, 29–42, and 43–56, (i) = (coel), (i) = (tiss), and (i) = (cali), respectively (Eq. A5).

$$r_{(1:14)};r_{(15:28)};r_{(29:42)};r_{(43:56)} = \begin{bmatrix} k_{+1}\cdot \mathrm{CO}_{2(i)} \\ k_{-1}\cdot \mathrm{HCO}_{3(i)}^{-}\cdot \mathrm{H}_{(i)}^{+} \\ k_{+4}\cdot \mathrm{CO}_{2(i)}\cdot \mathrm{OH}_{(i)}^{-} \\ k_{-4}\cdot \mathrm{HCO}_{3(i)}^{-} \\ k_{+5}^{\mathrm{H}^+}\cdot \mathrm{CO}_{3(i)}^{2-}\cdot \mathrm{H}_{(i)}^{+} \\ k_{-5}^{\mathrm{H}^+}\cdot \mathrm{HCO}_{3(i)}^{-} \\ k_{+5}^{\mathrm{OH}^-}\cdot \mathrm{HCO}_{3(i)}^{-}\cdot \mathrm{OH}_{(i)}^{-} \\ k_{-5}^{\mathrm{OH}^-}\cdot \mathrm{CO}_{3(i)}^{2-} \\ k_{+6} \\ k_{-6}\cdot \mathrm{H}_{(i)}^{+}\cdot \mathrm{OH}_{(i)}^{-} \\ k_{+7}\cdot \mathrm{B(OH)}_{3(i)}\cdot \mathrm{OH}_{(i)}^{-} \\ k_{-7}\cdot \mathrm{B(OH)}_{4(i)}^{-} \\ k_{+8}\cdot \mathrm{CO}_{3(i)}^{2-}\cdot \mathrm{B(OH)}_{3(i)} \\ k_{-8}\cdot \mathrm{B(OH)}_{4(i)}^{-}\cdot \mathrm{HCO}_{3(i)}^{-} \end{bmatrix} \quad \text{(A5)}$$

The flux of advective exchange of state variables between seawater and coelenteron is assumed to linearly depend on the concentration gradient between the two compart-

BGD
9, 2655–2689, 2012

ments with a constant exchange rate, ϖ (Eq. A6).

$$r_{(57:64)} = \begin{bmatrix} \varpi \cdot \left(CO_{2(sea)} - CO_{2(coel)}\right) \\ \varpi \cdot \left(HCO^{-}_{3(sea)} - HCO^{-}_{3(coel)}\right) \\ \varpi \cdot \left(CO^{2-}_{3(sea)} - CO^{2-}_{3(coel)}\right) \\ \varpi \cdot \left(H^{+}_{(sea)} - H^{+}_{(coel)}\right) \\ \varpi \cdot \left(OH^{-}_{(sea)} - OH^{-}_{(coel)}\right) \\ \varpi \cdot \left(B(OH)_{3(sea)} - B(OH)_{3(coel)}\right) \\ \varpi \cdot \left(B(OH)^{-}_{4(sea)} - B(OH)^{-}_{4(coel)}\right) \\ \varpi \cdot \left(Ca^{2+}_{(sea)} - Ca^{2+}_{(coel)}\right) \end{bmatrix} \quad \text{(A6)}$$

Diffusion of CO_2 over compartment boundaries is parameterized according to Fick's first law of diffusion, i.e. is assumed to be driven by the concentration gradient of CO_2 and the diffusion coefficient of CO_2 over eukaryotic cell membranes, D_{CO_2} (Eq. A7). CO_2 diffusion is considered over three boundary layers, the polyp surface facing the seawater, the surface facing the coelenteron, and the layer facing the calcifying fluid.

$$r_{(65:67)} = \begin{bmatrix} D_{CO_2} \cdot \left(CO_{2(sea)} - CO_{2(tiss)}\right) \\ D_{CO_2} \cdot \left(CO_{2(coel)} - CO_{2(tiss)}\right) \\ D_{CO_2} \cdot \left(CO_{2(tiss)} - CO_{2(cali)}\right) \end{bmatrix} \quad \text{(A7)}$$

Active bicarbonate uptake and transport over the three boundary layers of the polyp tissue are parameterized to follow simple Michaelis-Menten kinetics (Eq. A8). The maximum rate, $V_{HCO_{3(i)}}$, is assumed to be different for the three different pathways and therefore assigned different indices according to the compartment from which bicarbonate is removed. The half-saturation constant, k_{HCO_3}, is set to be equal for all three reactions. As active transport is assumed to only occur during light exposure, the Michaelis–Menten kinetics are multiplied with a factor, S, that acts as a light-switch

BGD
9, 2655–2689, 2012

and is either 0 or 1, depending on light conditions.

$$r_{(68:70)} = \begin{bmatrix} \mathcal{S} \cdot \left(\frac{V_{HCO_{3(sea)}} \cdot HCO^-_{3(sea)}}{k_{HCO_3} + HCO^-_{3(sea)}} \right) \\ \mathcal{S} \cdot \left(\frac{V_{HCO_{3(coel)}} \cdot HCO^-_{3(coel)}}{k_{HCO_3} + HCO^-_{3(coel)}} \right) \\ \mathcal{S} \cdot \left(\frac{V_{HCO_{3(tiss)}} \cdot HCO^-_{3(tiss)}}{k_{HCO_3} + HCO^-_{3(tiss)}} \right) \end{bmatrix} \quad \text{(A8)}$$

Calcium transport is also realized following Michaelis-Menten kinetics (Eq. A9). Half-saturation constants, k_{Ca}, are again assumed to be the same for all passages, whereas maximum rates, $V_{Ca_{(i)}}$, are assumed to differ. Multiplication with the light-switch, $\mathcal{S}$, turns active transport on and off, according to light situations.

$$r_{(71:73)} = \begin{bmatrix} \mathcal{S} \cdot \left(\frac{V_{Ca_{(sea)}} \cdot Ca^{2+}_{(sea)}}{k_{Ca} + Ca^{2+}_{(sea)}} \right) \\ \mathcal{S} \cdot \left(\frac{V_{Ca_{(coel)}} \cdot Ca^{2+}_{(coel)}}{k_{Ca} + Ca^{2+}_{(coel)}} \right) \\ \mathcal{S} \cdot \left(\frac{V_{Ca_{(tiss)}} \cdot Ca^{2+}_{(tiss)}}{k_{Ca} + Ca^{2+}_{(tiss)}} \right) \end{bmatrix} \quad \text{(A9)}$$

Photosynthesis and respiration are implemented as constant fluxes of either consumption or production of CO_2 in the coral tissue. The constant rates, C_{phot} and C_{resp}, are multiplied with the light-switch, $\mathcal{S}$, or $1-\mathcal{S}$, to assure that photosynthesis occurs only during light phases and respiration only occurs in the dark (Eq. A10).

$$r_{(74:75)} = \begin{bmatrix} \mathcal{S} \cdot C_{phot} \\ (1-\mathcal{S}) \cdot C_{resp} \end{bmatrix} \quad \text{(A10)}$$

Calcification is implemented according to the equation proposed by Zuddas and Mucci (1994) (Eq. A11).

$$r_{(76)} = \left[k_p \cdot (\Omega_{(cali)} - 1)^n \right] \quad \text{(A11)}$$

BGD
9, 2655–2689, 2012

The saturation state of the calcifying fluid, $\Omega_{(cali)}$, with respect to aragonite is defined by the ion product of calcium and carbonate, divided by the solubility product of aragonite, K^*_{sp} (Eq. A12). K^*_{sp} of aragonite is calculated according to Zeebe and Wolf-Gladrow (2001).

$$\Omega_{(cali)} = \frac{Ca^{2+}_{(cali)} \cdot CO^{2-}_{3(cali)}}{K^*_{sp}} \quad \text{(A12)}$$

Acknowledgements. This study was fully funded by and conducted at the Leibniz Center for Tropical Marine Ecology (ZMT) in Bremen, Germany. We intend this work as a contribution to the European Project of Ocean Acidification (EPOCA), which received funding from the European Community's Seventh Framework Programme (FP7/2007-2013) under grant agreement no. 211384.

References

Al-Horani, F. A., Al-Moghrabi, S. M., and De Beer, D.: The mechanism of calcification and its relation to photosynthesis and respiration in the scleractinian coral *Galaxea fascicularis*, Mar. Biol., 142, 419–426, doi:10.1007/s00227-002-0981-8, 2003. 2658, 2660, 2661, 2666, 2669, 2670

Allemand, D., Ferrierpages, C., Furla, P., Houlbreque, F., Puverel, S., Reynaud, S., Tambutté, E., Tambutté, S., and Zoccola, D.: Biomineralisation in reef-building corals: from molecular mechanisms to environmental control, C.R. Palevol, 3, 453–467, doi:10.1016/j.crpv.2004.07.011, 2004. 2658, 2659, 2666

Anthony, K. R. N., Kline, D. I., Diaz-Pulido, G., Dove, S., and Hoegh-Guldberg, O.: Ocean acidification causes bleaching and productivity loss in coral reef builders, P. Natl. Acad. Sci. USA, 105, 17442–17446, doi:10.1073/pnas.0804478105, 2008. 2670

Caldeira, K. and Wickett, M. E.: Anthropogenic carbon and ocean pH, Nature, 425, 365, 2003. 2657

Cohen, A. L. and Holcomb, M.: Why corals care about ocean acidification: uncovering the mechanism, Oceanography, 22, 118–127, 2009. 2657

BGD
9, 2655–2689, 2012

Doney, S. C., Fabry, V. J., Feely, R. A., and Kleypas, J. A.: Ocean acidification: the other CO_2 problem, Annu. Rev. Mar. Sci., 1, 169–192, doi:10.1146/annurev.marine.010908.163834, 2009. 2657

Furla, P., Galgani, I., Durand, I., and Allemand, D.: Sources and mechanisms of inorganic carbon transport for coral calcification and photosynthesis, J. Exp. Biol., 3457, 3445–3457, 2000. 2660, 2666, 2667, 2668, 2669, 2670

Gattuso, J.-P., Allemand, D., and Frankignoulle, M.: Photosynthesis and calcification at cellular, organismal and community levels in coral reefs: a review on interactions and control by carbonate chemistry, Am. Zool., 39, 160–183, doi:10.1093/icb/39.1.160, 1999. 2669

Gehlen, M., Gangstø, R., Schneider, B., Bopp, L., Aumont, O., and Ethe, C.: The fate of pelagic $CaCO_3$ production in a high CO_2 ocean: a model study, Biogeosciences, 4, 505–519, doi:10.5194/bg-4-505-2007, 2007. 2671

Gould, G. W., East, J. M., Froud, R. J., McWhirter, J. M., Stefanova, H. I., and Lee, A. G.: A kinetic model for the $Ca^{2+} + Mg^{2+}$-activated ATPase of sarcoplasmic reticulum, Biochem. J., 237, 217–227, 1986. 2658

Iglesias-Prieto, R., Matta, J. L., Robins, W. A., and Trench, R. K.: Photosynthetic response to elevated temperature in the symbiotic dinoflagellate *Symbiodinium microadriaticum* in culture, P. Natl. Acad. Sci. USA, 89, 10302–10305, 1992. 2670

Ip, Y. K., Lim, A. L. L., and Lim, R. W. L.: Some properties of calcium-activated adenosine triphosphatase from the hermatypic coral *Galaxea fascicularis*, Mar. Biol., 111, 191–197, 1991. 2659, 2666

IPCC: Climate change 2007: Synthesis Report. Contribution of Working Groups I, II and III to the Fourth Assessment Report of the Intergovernmental Panel on Climate Change, Tech. rep., edited by: Pachauri, R. K. and Reisinger, A. [Core Writing Team], IPCC, Geneva, Switzerland, 2007. 2656

Kleypas, J. A., Buddemeier, R. W., and Gattuso, J.-P.: The future of coral reefs in an age of global change, Int. J. Earth Sci., 90, 426–437, doi:10.1007/s005310000125, 2001. 2657

Kleypas, J. A., McManus, J. W., and Meñez, L. A. B.: Environmental limits to coral reef development: where do we draw the line?, Am. Zool., 39, 146–159, doi:10.1093/icb/39.1.146, 1999. 2670

Lasaga, A. C.: Kinetic Theory in Earth Sciences, Princeton University Press, Princeton, 1998. 2657

Leuzinger, S., Anthony, K. R. N., and Willis, B. L.: Reproductive energy investment in corals:

BGD
9, 2655–2689, 2012

scaling with module size, Oecologia, 136, 524–31, doi:10.1007/s00442-003-1305-5, 2003. 2661, 2669

Marshall, A. T. and Clode, P.: Calcification rate and the effect of temperature in a zooxanthellate and an azooxanthellate scleractinian reef coral, Coral Reefs, 23, 218–224, doi:10.1007/s00338-004-0369-y, 2004. 2670

Marubini, F., Barnett, H., Langdon, C., and Atkinson, M. J.: Dependence of calcification on light and carbonate ion concentration for the hermatypic coral *Porites compressa*, Mar. Ecol.-Prog. Ser., 220, 153–162, doi:10.3354/meps220153, 2001. 2658

Marubini, F., Ferrier-Pages, C., Furla, P., and Allemand, D.: Coral calcification responds to seawater acidification: a working hypothesis towards a physiological mechanism, Coral Reefs, 27, 491–499, doi:10.1007/s00338-008-0375-6, 2008. 2665, 2666, 2667

Orr, J. C., Fabry, V. J., Aumont, O., Bopp, L., Doney, S. C., Feely, R. A., Gnanadesikan, A., Gruber, N., Ishida, A., Joos, F., Key, R. M., Lindsay, K., Maier-Reimer, E., Matear, R., Monfray, P., Mouchet, A., Najjar, R. G., Plattner, G.-K., Rodgers, K. B., Sabine, C. L., Sarmiento, J. L., Schlitzer, R., Slater, R. D., Totterdell, I. J., Weirig, M.-F., Yamanaka, Y., and Yool, A.: Anthropogenic ocean acidification over the twenty-first century and its impact on calcifying organisms, Nature, 437, 681–686, doi:10.1038/nature04095, 2005. 2657

Pytkowicz, R. M.: Calcium carbonate retention in supersaturated seawater, Am. J. Sci., 273, 515, 1973. 2657

Ridgwell, A., Schmidt, D. N., Turley, C., Brownlee, C., Maldonado, M. T., Tortell, P., and Young, J. R.: From laboratory manipulations to Earth system models: scaling calcification impacts of ocean acidification, Biogeosciences, 6, 2611–2623, doi:10.5194/bg-6-2611-2009, 2009. 2657

Riebesell, U., Fabry, V., Hansson, L., and Gattuso, J.-P.: Guide to best practices for ocean acidification research and data reporting, Tech. rep., Publications Office of the European Union, Luxembourg, 2009. 2666

Ries, J. B.: A physicochemical framework for interpreting the biological calcification response to CO_2-induced ocean acidification, Geochim. Cosmochim. Ac., 75, 4053–4064, doi:10.1016/j.gca.2011.04.025, 2011. 2658, 2667

Ries, J. B., Cohen, A. L., and McCorkle, D. C.: Marine calcifiers exhibit mixed responses to CO_2-induced ocean acidification, Geology, 37, 1131–1134, doi:10.1130/G30210A.1, 2009. 2657, 2667

Sabine, C. L., Feely, R. A., Gruber, N., Key, R. M., Lee, K., Bullister, J. L., Wanninkhof, R.,

BGD
9, 2655–2689, 2012

Wong, C. S., Wallace, D. W. R., Tilbrook, B., Millero, F. J., Peng, T.-H., Kozyr, A., Ono, T., and Rios, A. F.: The oceanic sink for anthropogenic CO_2, Science, 305, 367–71, doi:10.1126/science.1097403, 2004. 2656

Sueltemeyer, D. and Rinast, K.-A.: The CO_2 permeability of the plasma membrane of *Chlamydomonas reinhardtii*: mass-spectrometric ^{18}O-exchange measurements from $^{13}C^{18}O_2$ in suspensions of carbonic anhydrase-loaded plasma-membrane vesicles, Planta, 200, 358–368, doi:10.1007/BF00200304, 1996. 2659

Tambutté, E., Allemand, D., Mueller, E., and Jaubert, J.: A compartmental approach to the mechanism of calcification in hermatypic corals, J. Exp. Biol., 199, 1029–1041, 1996. 2658

Wanninkhof, R.: Relationship between wind speed and gas exchange over the ocean, J. Geophys. Res., 97, 7373–7382, 1992. 2659

Wolf-Gladrow, D. A., Zeebe, R. E., Klaas, C., Körtzinger, A., and Dickson, A. G.: Total alkalinity: the explicit conservative expression and its application to biogeochemical processes, Mar. Chem., 106, 287–300, 2007. 2661

Zeebe, R. E. and Wolf-Gladrow, D. A.: CO_2 in Seawater: Equilibrium, Kinetics, Isotopes, Vol. 65 of Elsevier Oceanography Book Series, 1st edn., Elsevier, Amsterdam, 2001. 2657, 2659, 2666, 2673, 2676

Zoccola, D., Tambutté, E., Kulhanek, E., Puverel, S., Scimeca, J.-C., Allemand, D., and Tambutté, S.: Molecular cloning and localization of a PMCA P-type calcium ATPase from the coral *Stylophora pistillata*, Biochim. Biophys. Acta, 1663, 117–126, doi:10.1016/j.bbamem.2004.02.010, 2004. 2659, 2667

Zuddas, P. and Mucci, A.: Kinetics of calcite precipitation from seawater: I. A classical chemical kinetics description for strong electrolyte solutions, Geochim. Cosmochim. Ac., 58, 4353–4362, doi:10.1016/0016-7037(94)90339-5, 1994. 2659, 2675

BGD
9, 2655–2689, 2012

Table 1. Initial concentrations of state variables.

State variable	Seawater	Coelenteron	Tissue	Calicoblastic layer	Unit
CO_2	9.5415×10^{-6}	9.5415×10^{-6}	9.5415×10^{-6}	6.5165×10^{-6}	mol kg^{-1}
HCO_3^-	2.0542×10^{-3}	2.0542×10^{-3}	2.0542×10^{-3}	1.403×10^{-3}	mol kg^{-1}
CO_3^{2-}	3.3622×10^{-4}	3.3622×10^{-4}	3.3622×10^{-4}	2.2963×10^{-4}	mol kg^{-1}
H^+	6.3096×10^{-9}	6.3096×10^{-9}	6.3096×10^{-9}	5.0119×10^{-10}	mol kg^{-1}
OH^-	6.8990×10^{-6}	6.8990×10^{-6}	6.8990×10^{-6}	8.6854×10^{-5}	mol kg^{-1}
H_2O	5.36×10^{1}	5.36×10^{1}	5.36×10^{1}	5.36×10^{1}	mol kg^{-1}
$B(OH)_4^-$	3.5534×10^{-4}	3.5534×10^{-4}	3.5534×10^{-4}	3.5534×10^{-4}	mol kg^{-1}
$B(OH)_3$	1.1981×10^{-4}	1.1981×10^{-4}	1.1981×10^{-4}	1.1981×10^{-4}	mol kg^{-1}
Ca^{2+}	1.0×10^{-2}	1.0×10^{-2}	1.0×10^{-2}	1.06×10^{-2}	mol kg^{-1}
$CaCO_3$	–	–	–	1.0×10^{-7}	mol kg^{-1}

BGD
9, 2655–2689, 2012

Table 2. Model parameters.

Variable	Definition	Value and unit
ω	exchange rate of advective transport	$3.33\,s^{-1}$
D_{CO_2}	diffusion coefficient for CO_2	$2.8 \times 10^{-3}\,cm\,s^{-1}$
$V_{HCO_{3(sea)}}$	maximum uptake rate for bicarbonate (sea-tiss)	$1500 \times 10^{-12}\,mol\,C\,mg\,prot^{-1}\,min^{-1}$
$V_{HCO_{3(coel)}}$	maximum uptake rate for bicarbonate (coel-tiss)	$1500 \times 10^{-12}\,mol\,C\,mg\,prot^{-1}\,min^{-1}$
$V_{HCO_{3(tiss)}}$	maximum transport rate for bicarbonate (tiss-cali)	$40.5 \times 10^{-12}\,mol\,C\,mg\,prot^{-1}\,min^{-1}$
k_{HCO_3}	half-saturation constant bicarbonate transport	$1.0 \times 10^{-3}\,mmol\,m^{-3}$
$V_{Ca_{(sea)}}$	maximum uptake rate for calcium (sea-tiss)	$0\,mol\,Ca\,mg\,prot^{-1}\,min^{-1}$
$V_{Ca_{(coel)}}$	maximum uptake rate for calcium (coel-tiss)	$341.25 \times 10^{-12}\,mol\,Ca\,mg\,prot^{-1}\,min^{-1}$
$V_{Ca_{(tiss)}}$	maximum transport rate for calcium (tiss-cali)	$42.9 \times 10^{-12}\,mol\,Ca\,mg\,prot^{-1}\,min^{-1}$
k_{Ca}	half-saturation constant calcium transport	$1 \times 10^{-3}\,mol\,L^{-3}$
C_{phot}	net photosynthesis rate	$4\,mmol\,m^{-3}\,s^{-1}$
C_{resp}	dark respiration rate	$2\,mmol\,m^{-3}\,s^{-1}$
S	light switch	0 or 1 (dimensionless)
k_p	reaction rate for mineralization	$2.77\,\mu mol\,m^{-2}\,h^{-1}$
n	empirical reaction order	2.35 (dimensionless)

BGD
9, 2655–2689, 2012

Table 3. Initial conditions of state variables for pCO_2 scenarios.

State variable	280 ppmv	380 ppmv	700 ppmv	1000 ppmv	Unit
$CO_{2(sea)}$	7.5021×10^{-6}	10.181×10^{-6}	18.755×10^{-6}	26.793×10^{-6}	mol kg^{-1}
$HCO^{-}_{3(sea)}$	1.5993×10^{-3}	1.7106×10^{-3}	1.9046×10^{-3}	1.9964×10^{-3}	mol kg^{-1}
$CO^{2-}_{3(sea)}$	2.7909×10^{-4}	2.3525×10^{-4}	1.5832×10^{-4}	1.2176×10^{-4}	mol kg^{-1}
$H^{+}_{(sea)}$	6.9727×10^{-9}	8.8471×10^{-9}	14.6386×10^{-9}	19.9480×10^{-9}	mol kg^{-1}
$OH^{-}_{(sea)}$	6.2429×10^{-6}	4.9203×10^{-6}	2.9736×10^{-6}	2.1822×10^{-6}	mol kg^{-1}
$B(OH)_{3(sea)}$	3.4210×10^{-4}	3.6368×10^{-4}	4.0088×10^{-4}	4.1829×10^{-4}	mol kg^{-1}
$B(OH)^{-}_{4(sea)}$	1.3305×10^{-4}	1.1147×10^{-4}	7.4269×10^{-5}	5.6859×10^{-5}	mol kg^{-1}

BGD
9, 2655–2689, 2012

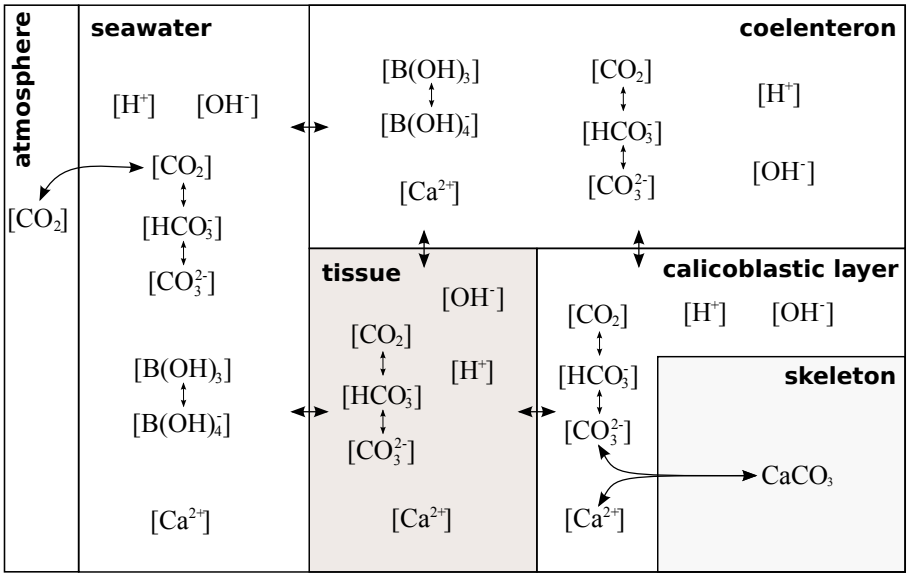

Fig. 1. Schematic of the coral polyp model. Four boxes are considered in the model (seawater, coelenteron, tissue, calicoblastic layer), which are interconnected via fluxes over the boundary layers. The seawater compartment is connected to an atmosphere with predefined pCO_2. Precipitation of the coral skeleton (calcification) occurs in the calicoblastic layer. State variables and fluxes are described in the text.

BGD
9, 2655–2689, 2012

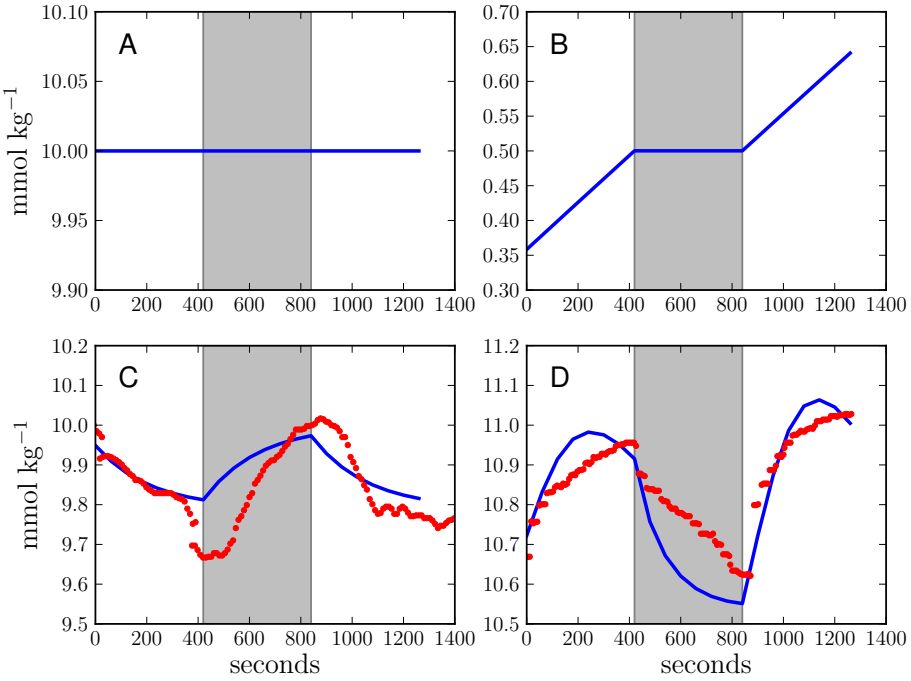

Fig. 2. Calcium ion concentrations in the four model compartments over time (A = seawater; B = tissue; C = coelenteron; D = calicoblastic layer). Data from microsensor studies by Al Horani et al. (2003) in red, model results in blue. Light periods from 0 to 420 s and from 840 s to the end. Dark period between 420 and 840 s.

BGD
9, 2655–2689, 2012

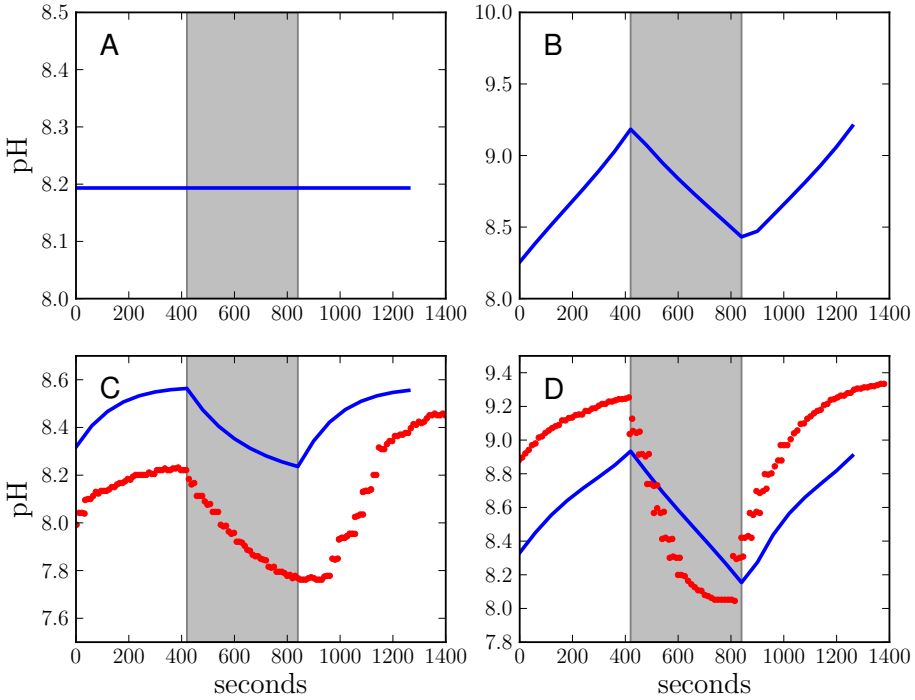

Fig. 3. pH in the four model compartments over time (A = seawater; B = tissue; C = coelenteron; D = calicoblastic layer). Data from microsensor studies by Al Horani et al. (2003) in red, model results in blue. Light periods from 0 to 420 s and from 840 s to the end. Dark period between 420 and 840 s.

BGD
9, 2655–2689, 2012

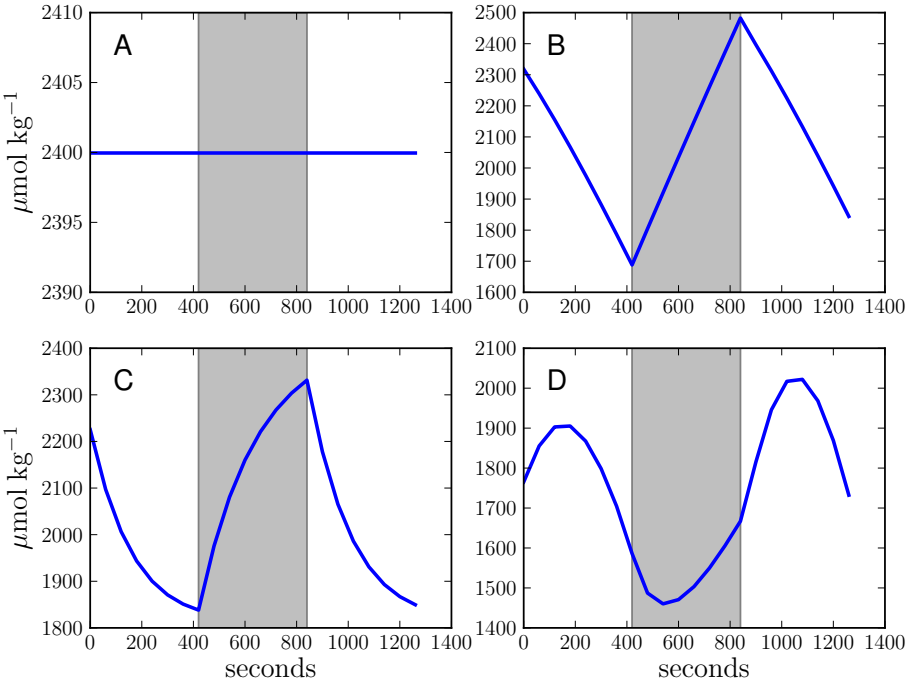

Fig. 4. DIC concentrations in the four model compartments over time (A = seawater; B = tissue; C = coelenteron; D = calicoblastic layer). The blue line shows the model results of the reference run. Light periods from 0 to 420 s and from 840 s to the end. Dark period between 420 and 840 s.

BGD
9, 2655–2689, 2012

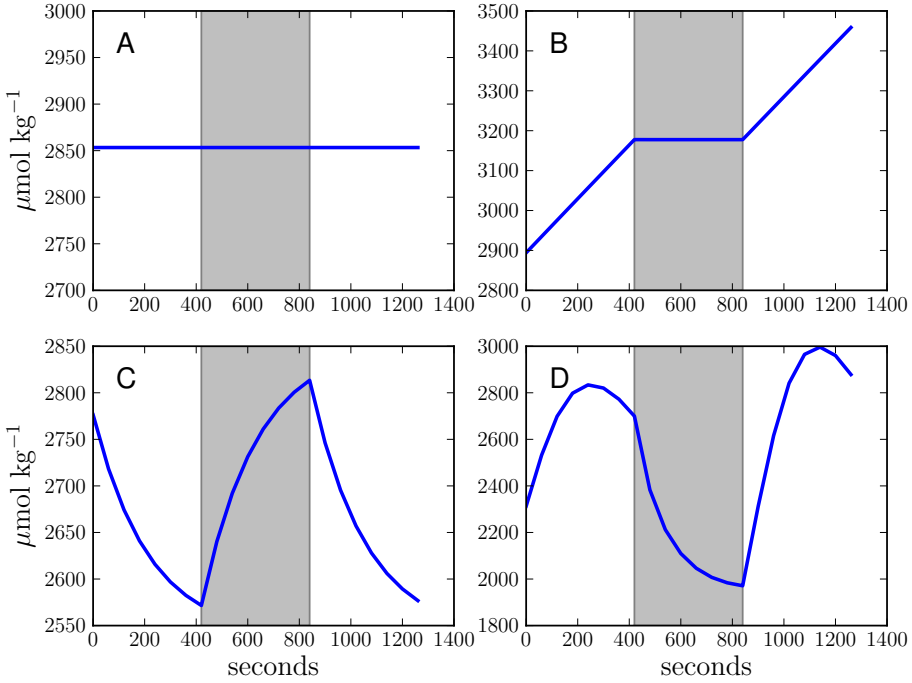

Fig. 5. Total alkalinity concentrations in the four model compartments over time (A = seawater; B = tissue; C = coelenteron; D = calicoblastic layer). The blue line shows the model results of the reference run. Light periods from 0 to 420 s and from 840 s to the end. Dark period between 420 and 840 s.

BGD
9, 2655–2689, 2012

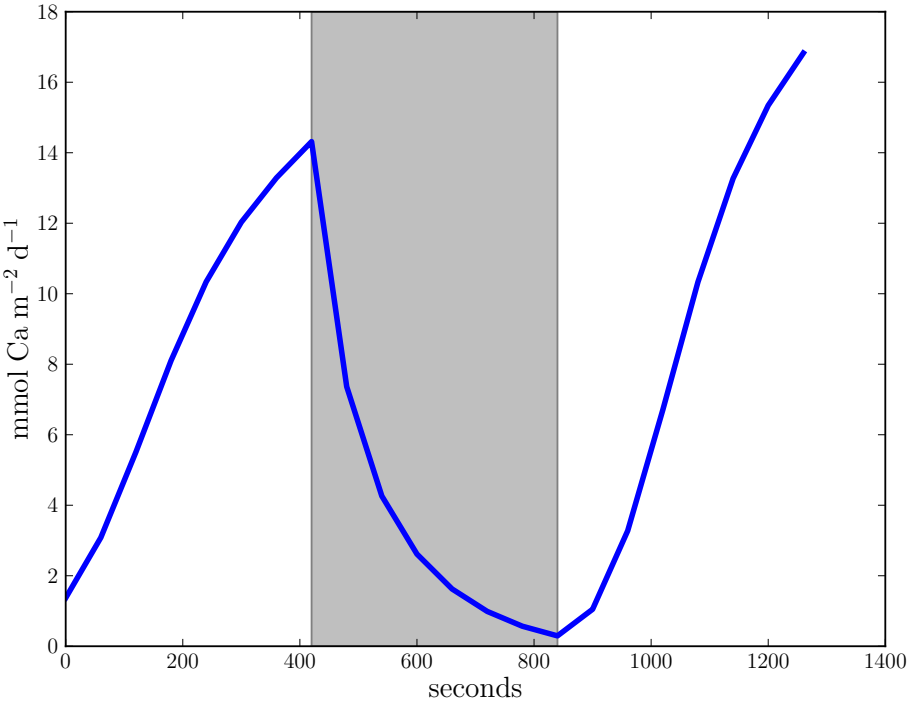

Fig. 6. Net calcification rate over time. Light periods from 0 to 420 s and from 840 s to the end. Dark period between 420 and 840 s.

BGD
9, 2655–2689, 2012

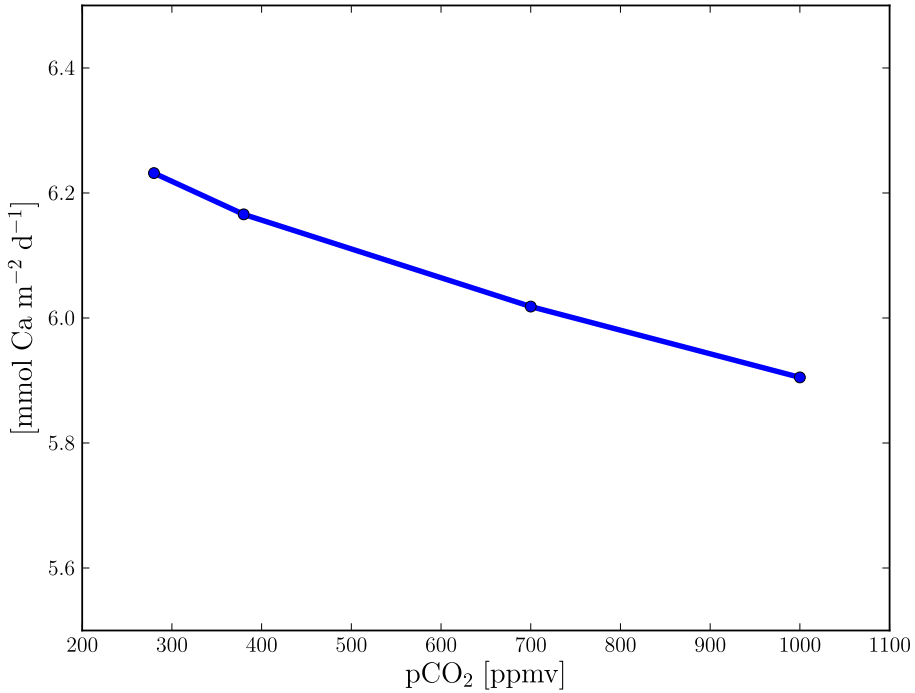

Fig. 7. Effect of changing seawater pCO_2 on the average coral calcification rate.

BGD
9, 2655–2689, 2012